J. Phys. B: At. Mol. Opt. Phys. **44** (2011) 175601 (8pp) doi:10.1088/0953-4075/44/17/175601

Selection rules in the few-photon double ionization of the helium atom

Hongcheng Ni[1], Shaohao Chen[1], Camilo Ruiz[2] and Andreas Becker[1]

[1] JILA and Department of Physics, University of Colorado, Boulder, CO 80309-0440, USA
[2] Centro de Laseres Pulsados Ultraintensos Ultracortos (CLPU), Plaza de la Merced s/n, Salamanca 37006, Spain

E-mail: hongcheng.ni@colorado.edu and andreas.becker@colorado.edu

Received 11 May 2011, in final form 13 July 2011
Published 9 August 2011
Online at stacks.iop.org/JPhysB/44/175601

Abstract
We analyse selection rules for the emission of two electrons from the helium atom following the absorption of a few photons in an intense laser field. The rules arise, as generalization of the well-studied one-photon case, due to the symmetries of the accessible final states in the two-electron continuum. We show, in particular, that an increase in the number of absorbed photons leads to alternating suppression and non-suppression of the back-to-back emission of the two electrons. Results of numerical simulations using a model of the helium atom are in agreement with the theoretical predictions.

(Some figures in this article are in colour only in the electronic version)

1. Introduction

Few-body dynamics involving three (or more) particles coupled by the Coulomb interaction belong to the most fundamental processes in atomic and molecular physics. Among these few-body processes are the ionization of an atom (e.g., the hydrogen atom) by collisional impact with an electron [1] and the ejection of both electrons of an atom (e.g., the helium atom) following absorption of one [2], a few [3] or many photons [4]. In particular, the evolution of three (or more) Coulomb-interacting particles in the continuum after the break-up of the atomic or molecular system has been a topic of recurring interest over many years. Nowadays, detector technology enables researchers to detect the momenta of two or even more particles in coincidence and, hence, to measure the differential cross sections of few-body processes [5]. This development offers the chance for theorists to explore the importance of symmetry and Coulomb interactions in the energy and momentum exchange between the constituents of a few-body system interacting with charged particles or light.

Despite the complex dynamics of an interacting few-body system, the final-state distributions of the particles often show some general structures. In particular, prominent nodes in the distributions represent restrictions for the correlated momenta of the outgoing particles. These restrictions arise either due to the Coulomb repulsion between the charged particles or due to symmetries (spin, angular momentum, parity, etc) of the final state of the few-body process. In this respect, the break-up of an atomic or molecular system following the absorption of a single photon has been studied in detail. Selection rules for the correlated electron momenta arising from the symmetry of the final state have been established for the single-photon double ionization of the helium atom [6] and molecular hydrogen [7], as well as the general case of an N-particle break-up following photoionization [8].

Recent advances in laser technology, namely free-electron laser facilities [9–11] and high harmonic generation [12], make possible the observation of the few-photon double ionization of atoms and molecules [13, 14]. Frequencies and intensities of these new laser systems restrict the processes to the few-photon interaction regime, in which a small number of channels lead to the ejection of the two electrons (as opposed to nonsequential double ionization at Ti:sapphire laser wavelength, which involves the absorption of a large number of photons from the field and rescattering effects [4]). We may therefore expect that the final two-electron states in few-photon double ionization possess a few definite symmetries and that the well-established selection rules in the single-photon case can be applied to the few-photon interactions as well.

In this paper, we study the restrictions to the position and momentum distributions of the emitted electrons in the continuum following the few-photon double ionization of the helium atom from the ground state. To this end, we first

briefly discuss the application of the final-state selection rules, derived by Briggs and co-workers [6–8], to few-photon double ionization. We then make use of a model for the interaction of the helium atom [15] with a laser field to test our expectations in numerical simulations. In our simulations, we will, in particular, analyse double-ionization pathways in which up to four photons are absorbed simultaneously by the two electrons to overcome the double-ionization threshold.

2. Application of selection rules to few-photon double ionization

2.1. Selection rules

The symmetries of a state in the two-electron continuum can lead to nodes in the corresponding configuration space wavefunction and the correlated momentum distribution [6]. Preparation of a system in an initial state of given symmetry (e.g., the ground state) as well as the symmetry of the transition operator (e.g., photon absorption) limits the symmetries of the final states that can be accessed in a specific process [7]. If in a transition all accessible final states share one or more symmetries or final states of different symmetries lead to the same node(s), there are zero(s) in the differential cross sections of the corresponding process. These selection rules have been accurately studied in the theory of the single-photon double ionization of atoms and molecules and reproduced in experiments (for a review, see [2]).

In order to identify and apply selection rules for the double ionization of the helium atom by the absorption of a few photons, we first briefly review the relevant symmetries of the final states in the two-electron continuum, as discussed by Briggs and co-workers (see [6, 7] and references cited therein). For the specification of the nodes in the configuration space wavefunction and the correlated electron momentum distributions, we employ the position vectors $\boldsymbol{r}_1$ and $\boldsymbol{r}_2$ and the momentum vectors $\boldsymbol{k}_1$ and $\boldsymbol{k}_2$ of the two electrons as well as the Jacobi coordinates $\boldsymbol{r} = \boldsymbol{r}_1 - \boldsymbol{r}_2$ (relative coordinate) and $\boldsymbol{R} = (\boldsymbol{r}_1 + \boldsymbol{r}_2)/2$ (centre-of-mass coordinate) and the corresponding momentum vectors $\boldsymbol{p} = (\boldsymbol{k}_1 - \boldsymbol{k}_2)/2$ and $\boldsymbol{P} = \boldsymbol{k}_1 + \boldsymbol{k}_2$.[3] We will consider double ionization from the ground state of the helium atom in a linearly polarized laser field with polarization axis aligned along the quantization axis of the system, which is chosen to be the z-axis. Furthermore, energies of the photons will be small enough such that the photon absorption can be described by an electric dipole transition. Thus, the quantum numbers $M = 0$ (projection of the total angular momentum to the quantization axis) and $S = 0$ (total spin) do not change in the cases considered here.

For single-photon double ionization from the ground state of the helium atom, which is of $^1S^{even}$-symmetry, the transition into the two-electron continuum leads to exclusive population of the $^1P^{odd}$-state. In this case and for linear polarization, three selection rules have been identified leading to nodes in the correlated wavefunction and momentum distribution [6]. We analyse each of these selection rules in view of their application to the absorption of more than one photon by the atom.

(1) There is a node in the two-electron wavefunction and a corresponding vanishing contribution to the correlated momentum distributions for both $\boldsymbol{r}_1$ and $\boldsymbol{r}_2$ ($\boldsymbol{k}_1$ and $\boldsymbol{k}_2$) perpendicular to the quantization axis of the system (here, the polarization axis of the field) if the final state is of odd parity. Since in dipole transitions the parity of the state changes, this selection rules applies for the absorption of either an even or an odd number of photons from the field depending on the parity of the initial state of the system. Thus, in the case of double ionization from the ground state of the helium atom, we expect the corresponding node to show up for odd-photon processes.

(2) For final states with even S and odd parity (or odd S and even parity), there appears a node in the configuration space wavefunction (momentum distribution) for $\boldsymbol{r}_1 = -\boldsymbol{r}_2$ ($\boldsymbol{k}_1 = -\boldsymbol{k}_2$), which is equivalent to $\boldsymbol{R} = 0$ ($\boldsymbol{P} = 0$). Since the total spin quantum number S does not change, while the parity of the state does change in an electric dipole transition, the selection rules apply again either for an even-photon or an odd-photon process depending here on the total spin and the parity of the initial state. For few-photon double ionization from the helium ground state, the node appears, as in the case of selection rule (1), if the number of absorbed photons is odd.

(3) Another node exists for $r_1 = r_2$ ($k_1 = k_2$) and $\theta_1 = \pi - \theta_2$ for final states with even S, odd L and odd parity (or, odd S, even L and even parity). Concerning the total spin quantum number and the parity, the same considerations as in the case of selection rule (2) apply. Thus, for double ionization from the ground state (even S, even parity and even L), the node is expected to be present for the absorption of an odd number of photons.

In summary, these selection rules should lead to alternating suppression and non-suppression of electron emission for certain configurations in the two-electron continuum wavefunction and momentum distribution as the number of absorbed photons increases beyond 1. Our analysis is based on the assumption that the electron-field coupling is perturbative, which is justified for the parameter regime considered in the numerical simulations below [16]. We may however note that similar conclusions have been drawn based on an S-matrix analysis of the double ionization of the helium atom by simultaneous multiphoton absorption in the nonperturbative intensity and wavelength regime [17]. Note that we have restricted our discussion above to those selection rules which are relevant for the most significant case of the double ionization of the helium atom from the ground state in a linearly polarized laser pulse. This case will be considered in the numerical simulations below as well. For an initial state with different symmetry or a different choice of the field polarization, other or further symmetry rules may have to be considered.

[3] We use Hartree atomic units, $e = m_e = \hbar = 1$, throughout the paper unless stated otherwise.

2.2. Numerical model of the helium atom

Following initial achievements towards the solution of the full time-dependent Schrödinger equation for the helium atom interacting with an intense laser pulse in view of an analysis of nonsequential double ionization at optical and near-infrared laser wavelengths (see [18] and references therein), in recent years much theoretical interest has been devoted to the double ionization of atoms by the absorption of two photons (see [19–23] for most recent studies and references therein). In the case of the two-photon process, results for the total cross sections as well as for momentum distributions have been reported. In particular, the passage from a simultaneous absorption of the photons (and simultaneous ejection of the electrons) to sequential double ionization, in which the absorption of the first photon generates a singly charged ion before the absorption of the second photon leads to the removal of the second electron, has been studied.

We are interested in analysing the occurrence of nodes for particular configurations of the position and momentum vectors in the probability density and the momentum distributions in numerical simulations. To this end, we may make use of any (lower-dimensional) model which exhibits all or some of the above selection rules. Here, we employ a model for the helium atom in which the centre-of-mass motion of the two electrons is restricted to the polarization axis of the linearly polarized external laser field. The Hamiltonian of this two-electron model (in Jacobi coordinates) is given by [15]

$$H(Z,\rho,z;t) = \frac{P_Z^2}{4} + p_\rho^2 + p_z^2 - \frac{P_Z A_Z(t)}{c} + \frac{1}{\sqrt{\rho^2+z^2}} - \frac{2}{\sqrt{\rho^2/4+(Z+z/2)^2+a^2}} - \frac{2}{\sqrt{\rho^2/4+(Z-z/2)^2+a^2}}, \quad (1)$$

where a^2 is a soft-core parameter introduced to smoothen the Coulomb singularity in the numerical computations.

Our model restricts the centre-of-mass motion of the two electrons along the polarization direction but does not restrict the symmetry of the dipole transition operator. Thus, the considerations regarding the symmetries of the accessible final states discussed above apply in this model as well. In general, in our model the momentum components of the individual electron along the polarization direction differ and therefore both equal and unequal energy sharings occur. But, along $Z = 0$ and $P_Z = 0$ only equal energy sharing is present in the model. This coincides with the kinematics for the nodes according to selection rules (2) and (3), which are predicted to occur for equal energy sharing. Thus, for these two selection rules, the model captures the relevant dynamics. Selection rule (1) can occur for special cases of unequal momentum components in the transverse direction as well, which is not captured by the present model and is a restriction in view of the present analysis. Moreover, in our model, the node arising due to selection rule (3) coincides with that due to selection rule (2). Thus, in the remainder of the paper, we will mainly discuss our results in view of selection rule (2).

In the actual computations, the time-dependent Schrödinger equation of the two-electron model is solved using the Crank–Nicolson method. The initial ground state wavefunction $\Psi(Z,\rho,z,t=0)$ is computed through imaginary time propagation using a grid size of $\Delta\rho = \Delta z = \Delta Z = 0.3$ and $a^2 = 0.135$. The field-free ground state energies of the helium atom and helium ion are found to be -2.937 and -1.985, respectively, which are both close to the real values of -2.904 and -2. The propagation of the wavefunction in the field is conducted using a box size with $N_\rho = 300$, $N_z = 600$ and $N_Z = 300$ points in the respective directions. An absorbing boundary of the form $\cos^{1/6}\left(\frac{\pi}{2}\frac{|x-x_0|}{L}\right)$ with $|x| \geqslant |x_0|$, spanning 10% of the box size in a certain direction, is used. x_0 denotes the border of the boundary region and L its width.

3. Nodes in probability and momentum distributions

In this section, we present the results of a series of numerical simulations based on the model presented above. In our calculations, we change the wavelength and peak intensity of the laser pulse such that the double-ionization process can proceed via the simultaneous absorption of one up to four photons. The wavelengths are chosen such that the probability for sequential double ionization is small (or negligible) in each of the cases considered. In each of the computations, we use a $\sin^2$-pulse with a total length of six cycles.

3.1. One-photon double ionization

First, we consider a central laser wavelength of 14.32 nm and a peak intensity of $I_0 = 1 \times 10^{14}$ W cm^{-2}. At this wavelength, the photon energy of 3.182 au exceeds the double-ionization threshold of our model He atom and the two electrons can be emitted after the absorption of a single photon. Figure 1 shows snapshots of the probability density distribution $|\Psi(Z,z,\rho;t)|^2$ integrated over ρ (left-hand panels) or z (right-hand panels) at time $t = 10$ au after the end of the pulse. The plots in the column on the left show distributions in the Z–z plane (integrated over the ρ-coordinate). In these plots, the contributions at the centre ($z \approx Z \approx 0$) mainly correspond to the remaining population in the neutral helium atom after the interaction. This can be clearly seen from the comparison of the plots in the upper and lower panels in the left-hand column, since the He ground state contribution is removed in the results in the lower panel. The single ionized population is displayed along the diagonals, while the contributions to double ionization can be found in the regions in between the diagonals. We clearly see a node along $Z = 0$ in the distribution, as predicted by selection rule (2) and shown by Briggs and co-workers before [6]. In the previous analysis of single-photon double ionization usually asymptotic final states (in time-independent S-matrix calculations) were considered; the present results offer a time-dependent view. It is seen from the results in figures 1 and 2 (the latter shows the distributions at two later time instants) that the node is present as soon as the pulse is over.

The plots in the right-hand columns of figures 1 and 2 offer the complementary view of the Z–ρ distributions, integrated

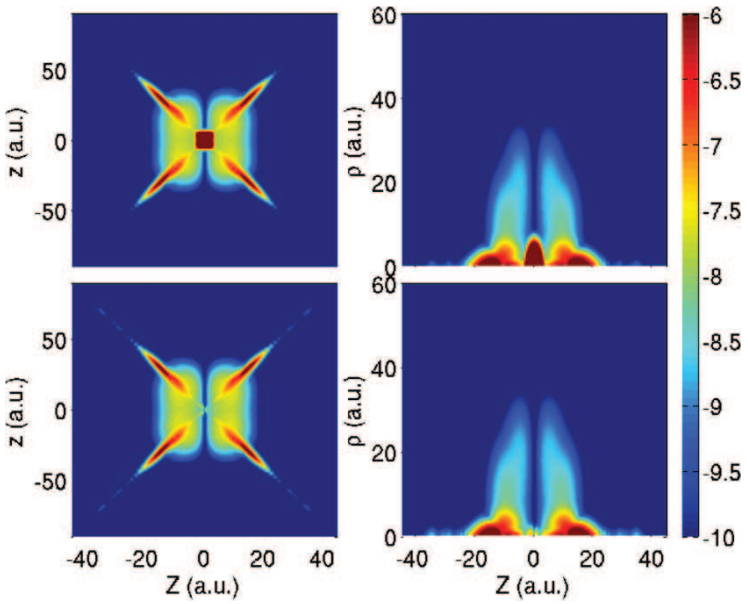

Figure 1. Probability density distribution (on a logarithmic scale) as a function of z and z (integrated over ρ, left-hand column) and as a function of ρ and z (integrated over z, right-hand column) following single-photon double ionization. In the results, presented in the panels in the lower row, the ground state wavefunction was removed before calculating the probability density distribution. The snapshots are taken at $t = 10$ au after the end of the laser pulses. Laser parameters: wavelength $\lambda = 14.32$ nm, peak intensity $I_0 = 1 \times 10^{14}$ W cm^{-2} and total pulse length six cycles.

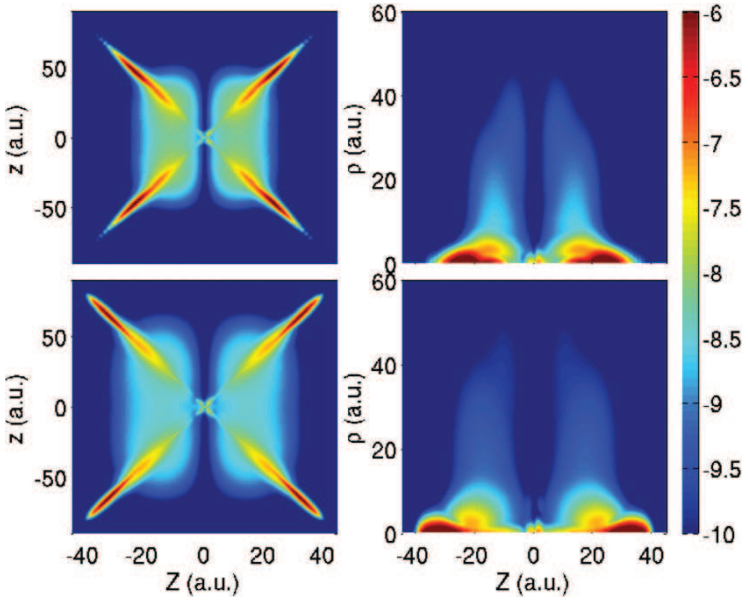

Figure 2. Same as figure 1 but at times $t = 20$ au (upper row) and $t = 30$ au (lower row). Shown are the probability density distributions after the removal of the He ground state from the full wavefunction.

over z. While the distributions at small ρ are mainly due to contributions from the neutral He atom and the He^+ ion, the population at large ρ indicates a highly correlated process, i.e. double ionization. Again, in all of the plots we see a node at $Z = 0$ for the contribution belonging to double ionization, as expected from selection rule (2) and the earlier work on single-photon double ionization [6].

3.2. Two-photon double ionization

Next, we consider two-photon double ionization, for which we expect that the node at $Z = 0$ is not present according to the selection rules. The simultaneous absorption of two photons does occur either as a second above-threshold double-ionization peak (ATDI, [17]) at higher intensities in the

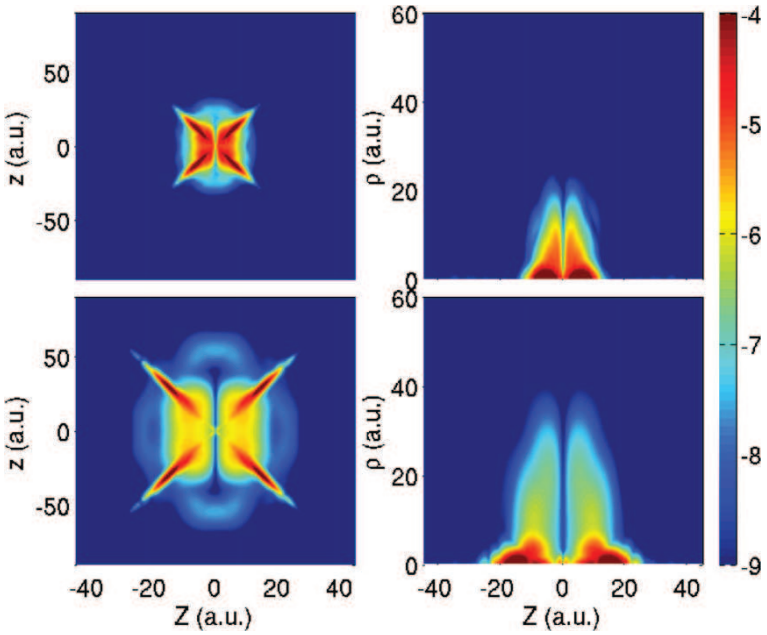

Figure 3. Probability density distribution (on a logarithmic scale) as a function of z and z (integrated over ρ, left-hand column) and as a function of ρ and z (integrated over z, right-hand column). The ground state wavefunction was removed before calculating the probability density distribution. The snapshots are taken at the end of the pulse (upper row) and $t = 10$ au after the pulse (lower row). Laser parameters: wavelength $\lambda = 14.32$ nm, peak intensity $I_0 = 1 \times 10^{16}$ W cm^{-2} and total pulse length six cycles.

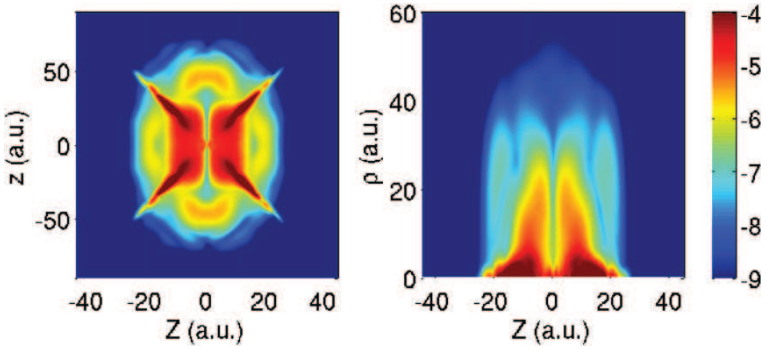

Figure 4. Same as figure 3, but at $I_0 = 1 \times 10^{17}$ W cm^{-2} and $t = 7.5$ au after the end of the pulse.

wavelength regime considered above, or at longer wavelengths at which the photon energy is smaller than the double-ionization threshold. In our simulations, we have analysed both cases.

First, we present in figure 3 results at the same wavelength as above but at a higher peak intensity of $I_0 = 1 \times 10^{16}$ W cm^{-2}. While in the z–Z distribution taken at the end of the pulse (panel in the upper-left corner) the evolving population in the double-ionization region does not show a clear structure, we can distinguish the contributions from single-photon and two-photon double ionization at some later time after the end of the pulse ($t = 10$ au, panel in the lower-left corner). Note that due to the difference in total kinetic energy, the single-photon contribution propagates at a smaller velocity than the two-photon contribution. Consequently, we find the latter contribution at larger distances from the centre of the z–Z distribution (i.e. the nucleus) than the one-photon distribution. Our expectations for the contribution along $Z = 0$ are obviously realized in the numerical results for the z–Z distribution (lower panel in the left-hand column): the absorption of two photons results in a maximum in the corresponding part of the distribution, while the node in the single-photon contribution is still present. In the Z–ρ distributions (panels in the right-hand column), there is no clear separation of the two processes possible and, hence, we observe a small population along $Z = 0$ due to the two-photon process.

Similar conclusions hold for the results at an even higher intensity of $I_0 = 1 \times 10^{17}$ W cm^{-2}, shown in figure 4. Here the contribution from the two-photon absorption (second ATDI peak) with a maximum along $Z = 0$ in the Z–z distribution is much stronger, as expected due to the nonlinearity of the

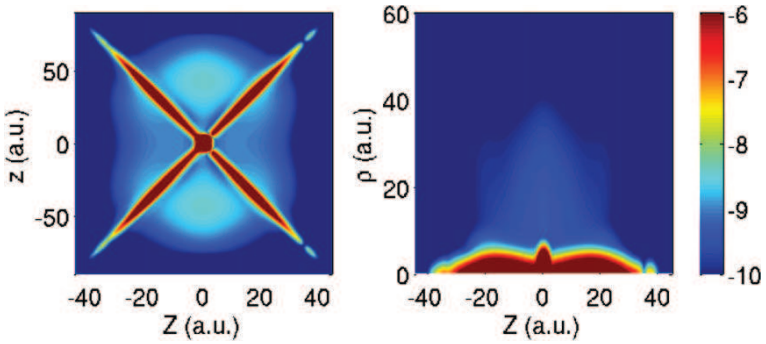

Figure 5. Probability density distribution (on a logarithmic scale) as a function of z and z (integrated over ρ, left-hand column) and as a function of ρ and z (integrated over z, right-hand column). The snapshots are taken $t = 30$ au after the pulse. Laser parameters: wavelength $\lambda = 28.64$ nm, peak intensity $I_0 = 1 \times 10^{14}$ W cm^{-2} and total pulse length six cycles.

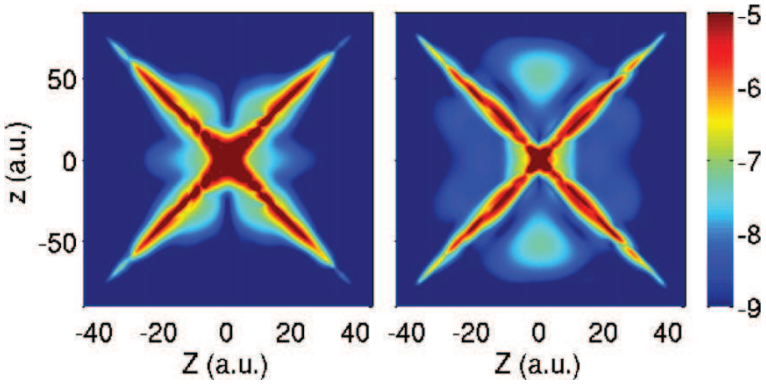

Figure 6. Probability density distribution (on a logarithmic scale) as a function of z and z (integrated over ρ). The snapshots are taken $t = 12.25$ au after the pulse. Laser parameters: wavelengths $\lambda = 42.96$ (left-hand column) and 57.28 nm (right-hand column), peak intensity $I_0 = 5 \times 10^{14}$ W cm^{-2} and total pulse length six cycles.

process. A clear separation of the single-photon process from the two-photon process is however no longer possible on the grid size used in the present simulations.

Next, we double the central wavelength of the laser field to $\lambda = 28.64$ nm (photon energy of 1.591 au). At this wavelength the (simultaneous) absorption of two photons is needed to overcome the double-ionization threshold. Note that the photon energy has been chosen such that a competing sequential double-ionization process requires the absorption of at least three photons and, hence, the corresponding contribution to the two-electron configuration space wavefunction is strongly suppressed. The results in figure 5 do not show a node along $Z = 0$ neither in the Z–z nor in the Z–ρ distribution, in agreement with selection rule (2) for a two-photon process from the He ground state. Instead, we observe as in the previous results in figures 3 and 4 a maximum in the contributions belonging to double ionization along this axis in the Z–z distribution. Note that the maximum indicates a preferential back-to-back emission of the two electrons at the present laser parameters, in agreement with recent observations in experiments on the two-photon double ionization of He [24] and Ne [25], as well as recent theoretical predictions [26].

3.3. Three- and four-photon double ionization

Finally, we consider double-ionization processes via the simultaneous absorption of more than two photons in order to verify (or, disprove) the alternating appearance of suppression and non-suppression of electron emission along the z-axis in the configuration space wavefunction for double ionization as the number of absorbed photons increases. We found that at longer wavelengths, the contributions of competing processes such as sequential double ionization are usually of similar (or even larger) strengths than the probability for the ejection of two electrons via the simultaneous absorption of photons. However, at specific wavelengths (and peak intensities), here 42.96 and 57.28 nm, we observe double ionization which arises from simultaneous three- and four-photon absorption. The results of the numerical simulations (see figure 6) clearly exhibit the suppression (for the odd-number-photon process) and the non-suppression (for the even-number-photon process) of electron emission along the $Z = 0$ axis in the Z–z distributions, as expected from selection rule (2).

3.4. Momentum distributions

As of now, we have demonstrated the selection rules in the configuration space of the two electrons. At the same time, the

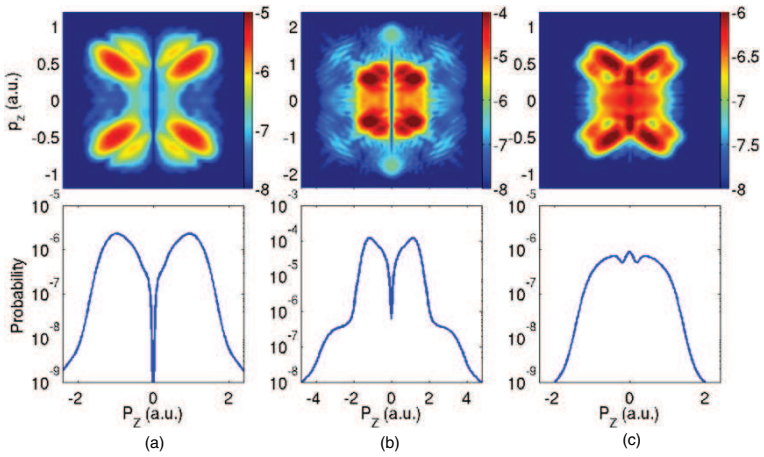

Figure 7. Correlated momentum distribution of p_z and P_Z (upper row) and momentum distribution in P_Z (lower row, integrated from upper row over p_z). Laser parameters: wavelengths $\lambda = 14.32$ (columns (a) and (b)) and 28.64 nm (column (c)), peak intensities $I_0 = 1 \times 10^{14}$ (columns (a) and (c)) and 1×10^{16} W cm^{-2} (column (b)) and total pulse length six cycles.

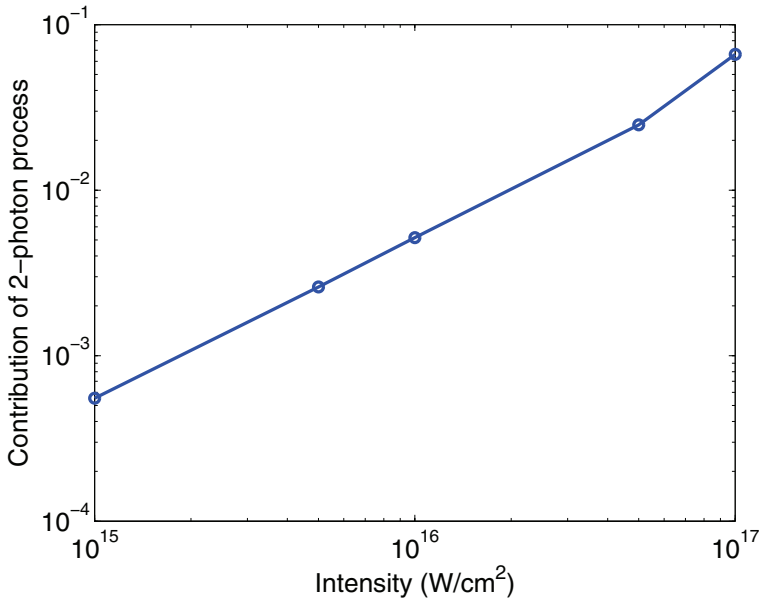

Figure 8. Ratio of the probability at $P_Z = 0$ to the maximum probability in the P_Z distributions as a function of intensity at a wavelength of 14.32 nm.

selection rules also apply to the momentum space distributions. As discussed above, when there is a node in the configuration space, there should be a corresponding node in the momentum space, and when there is an antinode in the configuration space, there should also be a corresponding antinode in the momentum space. Due to the lower dimensionality of our numerical model, we cannot provide quantitative predictions for the full momentum distributions but test certain aspects, here the existence of nodes.

Figure 7 shows correlated momentum distributions for the two electrons in the P_Z–p_z plane (upper row, integrated over the p_ρ direction) and along the P_Z-axis (lower row, integrated over both p_z and p_ρ). The momentum distributions are obtained by first separating the doubly ionized part of the configuration space wavefunction from the rest. To this end, we partition the coordinate space as [15]

$r_1 < 12$ and $r_2 < 12$: He atom

$r_1 < 6$ and $r_2 \geqslant 12$ or $r_1 \geqslant 12$ and $r_2 < 6$: He^+ ion

complementary space : He^{2+} ion,

where $r_{1,2} = \sqrt{\rho^2/4 + (Z \pm z/2)^2}$. Then, we project the doubly ionized part onto the final state wavefunction, which we approximate by a product state of a Coulomb wavefunction

in the relative coordinates ρ and z and a plane wave in the centre-of-mass coordinate z.

The momentum distributions displayed in the three columns correspond to the probability density distributions:

(a) in the lower row of figure 2, in which the single-photon process dominates,
(b) in the lower row of figure 3, in which both one- and two-photon processes are present, and
(c) in figure 5, in which the two-photon process is prominent.

It is obvious from the comparison of the results in figure 7 with the corresponding spatial distributions that both show the same nodes and antinodes. In particular, the nodes for the odd-number photon processes along $P_z = 0$ in the P_Z–p_z distributions (upper row of figure 7) can be clearly seen. We have found that the appearance of the nodes is insensitive to the method by which we extract the ionized population from the full wavefunction. It is also independent of how long the wavefunction is propagated after the end of the pulse and of the choice of the basis set for the two-electron continuum wavefunctions.

Comparing the momentum distributions in columns (a) and (b), we find that the contribution of the two-photon process increases with intensity at the wavelength of 14.32 nm. This can be quantified by the ratio of the probability at $P_Z = 0$ to the maximum probability in the P_Z distributions (lower row in figure 7), as shown in figure 8. One can see that the ratio increases almost linearly as a function of intensity. This is expected since the ratio basically represents the ratio between the probabilities for one- to two-photon absorption, which should follow the power law $I^2/I^1 = I^1$.

4. Conclusions

In summary, we showed that the well-known selection rules for single-photon double ionization can be generalized to the emission of two electrons following the simultaneous absorption of a few photons from an intense laser pulse. These selection rules, which arise due to the symmetries of the accessible final states in the two-electron continuum, correspond to nodes in the configuration space wavefunction and the correlated momentum distributions. In particular, the back-to-back emission of the two electrons is alternating either suppressed (forbidden) or non-suppressed as the number of absorbed photons increases. The theoretical predictions are tested well in numerical simulations using a model of the helium atom from the ground state. The numerical results for one- to four-photon double ionization clearly show the presence of the node in the back-to-back emission in the case of odd-number photon processes.

Acknowledgments

This work was supported by the US National Science Foundation.

References

[1] Rescigno T N, Baertschy M, Isaacs W A and McCurdy C W 1999 *Science* **286** 2474
[2] Briggs J S and Schmidt V 2000 *J. Phys. B: At. Mol. Opt. Phys.* **33** R1
[3] Rudenko A *et al* 2010 *J. Phys. B: At. Mol. Opt. Phys.* **43** 194004
[4] Becker A, Dörner R and Moshammer R 2005 *J. Phys. B: At. Mol. Opt. Phys.* **38** S753
[5] Ullrich J, Moshammer R, Dorn A, Dörner R, Schmidt L P H and Schmidt-Böcking H 2003 *Rep. Prog. Phys.* **66** 1463
[6] Maulbetsch F and Briggs J S 1995 *J. Phys. B: At. Mol. Opt. Phys.* **28** 551
[7] Walter M and Briggs J S 2000 *Phys. Rev. Lett.* **85** 1630
[8] Malcharek A W and Briggs J S 1997 *J. Phys. B: At. Mol. Opt. Phys.* **30** 4419
[9] Ackermann W *et al* 2007 *Nat. Photon.* **1** 336
[10] Shintake T *et al* 2008 *Nat. Photon.* **2** 555
[11] Emma P *et al* 2010 *Nat. Photon.* **4** 641
[12] Popmintchev T, Chen M-C, Arpin P, Murnane M M and Kapteyn H C 2010 *Nat. Photon.* **4** 822
[13] Nabekawa Y, Hasegawa H, Takahashi E J and Midorikawa K 2005 *Phys. Rev. Lett.* **94** 043001
[14] Kurka M *et al* 2010 *New J. Phys.* **12** 073305
[15] Ruiz C, Plaja L, Roso L and Becker A 2006 *Phys. Rev. Lett.* **96** 053001
[16] Makris M G, Lambropoulos P and Mihelič A 2009 *Phys. Rev. Lett.* **102** 033002
[17] Becker A and Faisal F H M 1994 *Phys. Rev.* A **50** 3256
Becker A and Faisal F H M 1994 *Phys. Rev.* A **51** 3390 (erratum)
[18] Parker J S, Doherty B J S, Taylor K T, Schultz K D, Blaga C I and DiMauro L F 2006 *Phys. Rev. Lett.* **96** 133001
[19] Bachau H 2011 *Phys. Rev.* A **83** 033403
[20] Palacios A, Horner D A, Rescigno T N and McCurdy C W 2010 *J. Phys. B: At. Mol. Opt. Phys.* **43** 194003
[21] Tao L, McCurdy C W and Rescigno T N 2010 *Phys. Rev.* A **82** 023423
[22] Nepstad R, Birkeland T and Førre M 2010 *Phys. Rev.* A **81** 063402
[23] Horner D A, Rescigno T N and McCurdy C W 2010 *Phys. Rev.* A **81** 023410
[24] Rudenko A *et al* 2008 *Phys. Rev. Lett.* **101** 073003
[25] Moshammer R *et al* 2007 *Phys. Rev. Lett.* **98** 203001
[26] Hu S X, Colgan J and Collins L A 2005 *J. Phys. B: At. Mol. Opt. Phys.* **38** L35